BMC Cell Biology

BioMed Central

Research article

# The pro-apoptotic Bcl-2 family member tBid localizes to mitochondrial contact sites

Michael Lutter[1,3], Guy A Perkins*[2,3] and Xiaodong Wang[1]

Address: [1]Howard Hughes Medical Institute and Department of Biochemistry, University of Texas Southwestern Medical Center, Dallas, TX 75235, USA, [2]The Department of Neurosciences and the National Center for Microscopy and Imaging Research, University of California, San Diego, La Jolla, CA 92093-0608, USA and [3] Contributed equally to this work

E-mail: Michael Lutter - michael.lutter@utsouthwestern.edu; Guy A Perkins* - perkins@ncmir.ucsd.edu; Xiaodong Wang - xwang@biochem.swmed.edu

*Corresponding author

Published: 8 November 2001

*BMC Cell Biology* 2001, **2**:22

Received: 27 September 2001
Accepted: 8 November 2001

This article is available from: http://www.biomedcentral.com/1471-2121/2/22



## Abstract

**Background:** Following cleavage by caspase 8, the C-terminus of Bid translocates from the cytosol to the mitochondria that is dependent upon structures formed by the mitochondrial-specific lipid cardiolipin. Once associated with mitochondria, truncated Bid (tBid) causes the potent release of cytochrome c, endonuclease G, and smac.

**Results:** We investigated whether tBid localizes specifically to the contact sites of mitochondria purported to be rich in cardiolipin. A point mutation changing the glycine at position 94 to glutamic acid in the BH3 domain of tBid ($tBid_{G94E}$) was principally used because mitochondria treated with this mutant tBid displayed better preservation of the outer membrane than those treated with wild type tBid. Additionally, $tBid_{G94E}$ lowers the cytochrome c releasing activity of tBid without affecting its targeting to mitochondria. Electron microscope tomography coupled with immunogold labeling was used as a new hybrid technique to investigate the three-dimensional distributions of tBid and $tBid_{G94E}$ around the mitochondrial periphery. The statistics of spatial point patterns was used to analyze the association of these proteins with contact sites.

**Conclusions:** Immunoelectron tomography with statistical analysis confirmed the preferential association of tBid with mitochondrial contact sites. These findings link these sites with cardiolipin in tBid targeting and suggest a role for Bcl-2 family members in regulating the activity of contact sites in relation to apoptosis. We propose a mechanism whereby Bcl-2 proteins alter mitochondrial function by disrupting cardiolipin containing contact site membranes.

## Background

Recent work has shown that the Bcl-2 family regulates mitochondrial homeostasis during apoptosis [1]. Pro-apoptotic members, including Bax, Bak, Bid, and Bim, promote the release of death-inducing proteins, such as cytochrome c [2,3], smac [4], and endonuclease G [5], from mitochondria while anti-apoptotic members, such as Bcl-2 and Bcl-$X_L$, inhibit this release. Following release into the cytosol, these death-inducing proteins promote apoptotic cell destruction through multiple pathways including caspase activation and nuclear DNA fragmentation.

In addition to controlling the release of pro-death proteins, the Bcl-2 family also alters the function of mitochondria undergoing apoptosis. Dysfunction of voltage dependent anion channel opening, ADP/ATP exchange, the electron transport chain, oxidative phosphorylation, and calcium buffering through the action of this family of proteins have been reported [6–8]. While early defects in the electron transport chain can be reversed by addition of exogenous cytochrome c, the damage eventually becomes refractory to cytochrome c addition [8]. This finding suggests that pro-death Bcl-2 proteins can damage mitochondrial function independent of cytochrome c loss.

Recently, we demonstrated that the targeting of the pro-apoptotic protein tBid to mitochondria depends upon the presence of the mitochondria-specific lipid cardiolipin in a possibly unique structure [9]. Cardiolipin has a defined distribution pattern within mitochondria [10]. It is found in high concentrations throughout the inner membrane, including at contact sites where the inner membrane and outer membrane interact. Cardiolipin is present at much lower concentrations elsewhere in the outer membrane. This distinction suggests that tBid might localize to contact sites because of the arrangement of cardiolipin there. To test this hypothesis, we determined the submitochondrial localization of tBid using a new hybrid technique – immunoelectron tomography, which couples conventional immunoelectron microscopy with tomography to add the third dimension. Tomographic analysis was chosen because it enables quantitative three-dimensional examination of fine structure within the relevant mitochondrial domains in semi-thick sections and thereby facilitates accurate representation of the sometimes complex membrane topology of this organelle [11,12]. Immunoelectron tomography is ideal for testing the independence of two types of labels, or label and structural component (as employed in this study), and their deviation from independence – colocalization or mutual inhibition – because it allows true 3-D distances to be measured. We report here an analysis of the 3-D distances of immunogold-labeled tBid from contact sites on the periphery of liver mitochondria that strongly supports the colocalization of the two.

## Results

Initially, we used wild type (WT) tBid that was myc-tagged for immunogold electron microscopy in our investigation of its localization along the mitochondrial periphery. Generally, WT tBid was observed to be in close proximity to contact sites (Fig. 1). However, the preservation of the outer membrane of isolated mouse liver mitochondria treated with this tBid was less than optimal for testing the hypothesis of tBid association with contact sites. A significant portion of the outer membrane was absent in most mitochondria observed, which may have been caused in part by the activity of this pro-apoptotic protein in releasing cytochrome c from the region between the outer and inner membranes. Neither was the gold labeling very high, most likely because a stripped outer membrane results in considerably fewer contact sites. Another pitfall was the use of 10-nm gold (as opposed to 5-nm gold) particles, which resulted in streaks that sometimes obscured the peripheral membranes (Fig. 1b). Even though harder to see in the microscope, for our analysis of mutant tBid labeling, we resorted to the smaller-sized gold, which greatly diminished the artifactual streaking.

To enhance mitochondrial membrane preservation, a point mutation changing the glycine residue at position 94 to glutamic acid in the BH3 domain of tBid was used. This mutation was previously shown to lower the cytochrome c releasing activity of tBid without affecting its targeting to mitochondria [3]. Mitochondria treated with $tBid_{G94E}$ displayed better preservation of the outer membrane than those treated with WT tBid. Hence, because of better preservation of contact sites, the $tBid_{G94E}$ was used primarily for the tomographic analysis. For immunogold labeling, a three-myc tag was placed at residue 67 of $Bid_{G94E}$. Following cleavage by caspase 8, a version of $tBid_{G94E}$ was generated with the three-myc tag at the N-terminus of $tBid_{G94E}$. Monoclonal anti-myc antibody was used for immunogold labeling to ensure high specificity of binding.

Before performing the time-expensive tomography, analysis of thin sections with conventional electron microscopy was used to judge the immunogold labeling quality. As expected, the number of gold particles per mitochondrion varied. However, most had several particles arrayed along the perimeter (Fig. 2). To confirm the specificity of labeling, three controls were analyzed by thin-section microscopy. Neither the no-primary control (Fig. 2) nor the second control, consisting of replacing the primary antibody with an excess of $tBid_{G94E}$ (data not shown), showed any gold particles. The third control was the presence of a contaminant organelle, peroxisomes (Fig. 2); no gold particles were observed attached to them. All three controls for labeling specificity indicated that the non-specific immunogold background was very low. Further, on those mitochondrial surfaces where the outer membrane was inadvertently stripped off during the specimen processing, no gold was observed, which is to be expected as there is no contact site where there is no outer membrane.

Electron tomography has several advantages over conventional two-dimensional immunogold electron micro-

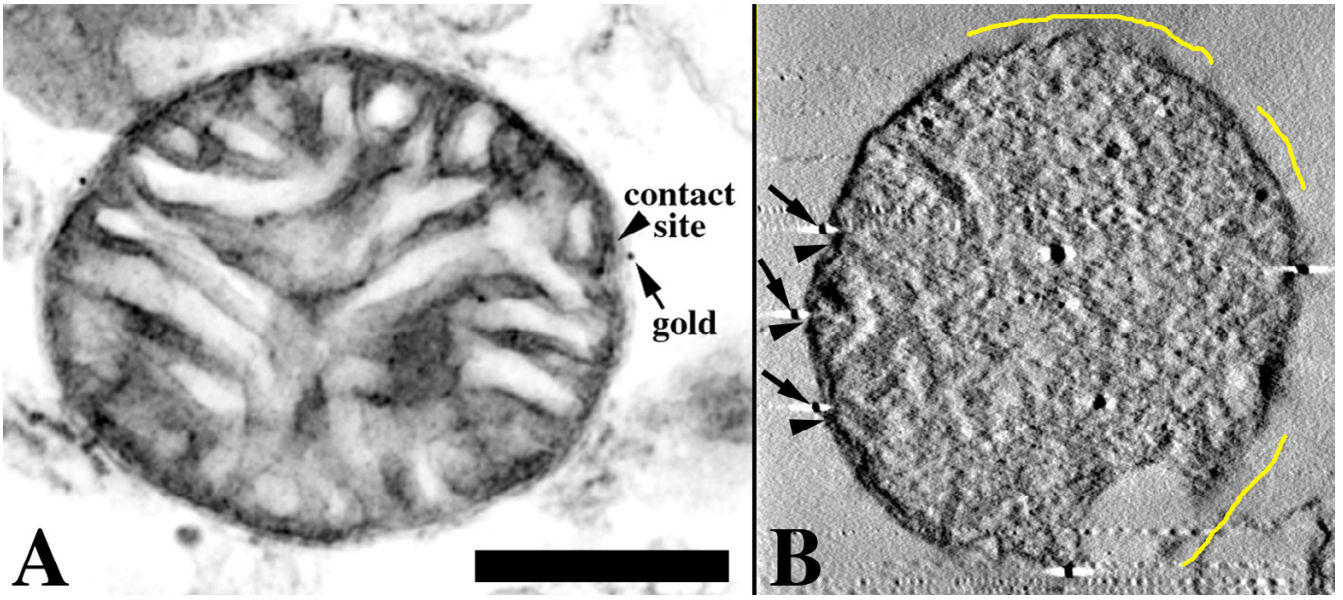


**Figure 1**
Isolated mouse liver mitochondrion treated with wild type tBid and labeled with 10 nm immunogold particles. **a)** Electron micrographs of thin sections (~50 nm thick) were examined to ascertain the quality of ultrastructural preservation and immunogold labeling density. On occasion, contact sites were observed; in these situations, a gold particle appeared to be nearby. For the most part, mitochondria treated with this tBid displayed rather poor preservation of the outer membrane, which may be a reflection of the activity of this pro-apoptotic protein in causing cytochrome c release. Neither was the gold labeling very high, most likely because a stripped outer membrane represents considerably fewer contact sites.**b)** One slice through a tomographic reconstruction showing partial stripping of the outer membrane. Largely, WT tBid was observed to be in close proximity to contact sites. Examples are indicated by arrows (gold particle) and arrowheads (contact site). Yellow traces indicate regions around the periphery where the outer membrane was stripped away. This mitochondrion is more in the orthodox state [33] than most observed. Horizontal streaks were caused by reconstructing the electron-dense gold particles and sometimes obscure features (bottom of image). Scale bars: (a), (b), 300 nm.

scopy that should be enumerated to understand the accuracy of the measurements made in this study. First, a more accurate localization of the 5-nm gold particles is possible because each slice of the tomographic reconstruction is about 2 nm in thickness compared with the typical 50–100 nm thickness used in conventional immuno-electron microscopy. Second, because the dimensions of contact sites (~14 nm diameter) [13,14] are considerably smaller than 50–100 nm, they are easily missed in conventional microscopy; this problem was removed by the typically finer sampling of electron tomography (~2 nm). Third, because tomography is inherently a 3-D tool, the 3-D placement of gold-labeled $tBid_{G94E}$ was obtained in relation to the 3-D distribution of contact sites and gold beads at high resolution. Unlike two-dimensional electron micrographs, true Euclidean distance was measured at a resolution of 4 nm (twice the pixel size, or thickness, according to Shannon sampling theory) in tomographic reconstructions from each gold bead to the nearest contact site. These measurements were then used for a statistical analysis of association.

Tomographic reconstruction of immunogold-labeled semi-thick sections confirmed the preferential association of tBid with contact sites. Figure 3 highlights features of a tomographic reconstruction of one of the $tBid_{G94E}$-labeled liver mitochondrion used in the statistical analysis. The mitochondrial volume sliced in three perpendicular planes where gold particles can be seen in all three faces (Fig. 3a, arrowheads) emphasizes the vast 3-D information available with tomography. Individual 2-nm slices illustrate how gold particles and contact sites can be easily identified with this hybrid, high-resolution technique (Fig. 3b). The insets in figure 3b show two examples of gold particles near contact sites. Graphic representations of a segmented volume are shown in figure 3c. Segmentation is a visual tool that defines and dissects volumes and thus aids the interpretation and measurement of structural interrelationships [15]. Once segmented, volumes were surface-rendered. With the surface-rendered volume, the various components of interest can be oriented to best study the proximity of gold and contact sites in relation to the membrane topology. A wealth of information can be quickly taken in by rotat-

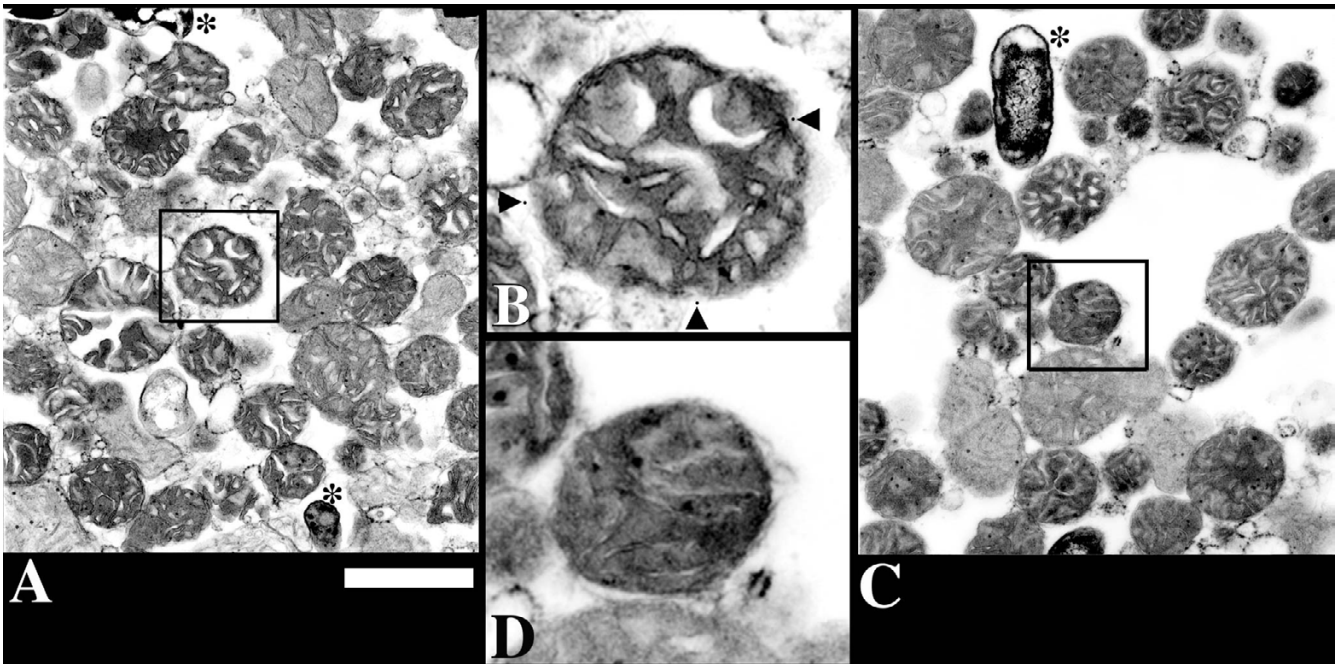


**Figure 2**
Conventional electron micrographs of thin sections of liver mitochondria assayed the quality of $tBid_{G94E}$ labelling. **a)** Section of pelleted mitochondria decorated with immunogold $tBid_{G94E}$. Most of the mitochondria are in the condensed state [33]. No difference in the general number of gold particles between condensed and orthodox mitochondria was observed. Peroxisome contamination indicated by asterisks in (a) and (c) had no immunogold background labeling.**b)** Mitochondrion boxed in (a) magnified 3x in order to visualize the 5-nm gold particles (arrowheads). **c)** No-primary control section showing little, if any, non-specific immunogold labeling on mitochondria treated with gold-conjugated secondary antibody.**d)** Mitochondrion boxed in (c) magnified 3x in order to show that there is no gold around the perimeter. Scale bars: (a), (c), 1000 nm.

ing the segmented volumes [http://ncmir.ucsd.edu/~perkins/tBid] . For example, it became apparent that contact sites can be clustered (Fig. 3c, right-hand side of mitochondrion).

We tested the association of tBid with contact sites by employing the statistics of spatial point patterns [16]. We measured the distances between the 3-D loci of all contact sites and immunogold particles in the tomographic reconstructions of WT tBid and $tBid_{G94E}$ labeled mitochondria. The closest contact site to each particle was calculated in Euclidean (3-D) space. Table 1 shows a comparison of experimental "nearest neighbors" with nearest neighbors expected from a random distribution of gold. The experimental mean value for nearest contact sites was significantly less than the random mean value for all mitochondria. We conducted a Student's t-test to test the null hypothesis that the experimental mean values would be reasonably likely to be obtained from sampling randomly. The probability of this test for "WT tBid 1" was $7.7 \times 10^{-6}$ and was even lower for the other samples. Thus, at essentially any significance level, the null hypothesis is rejected and we conclude that the association of tBid with contact sites is not random. For an understanding of what constitutes "close association" of gold particle with contact site, it is important to consider that the finite size of immunoglobulin molecules is about 8–10 nm in the most extended state. Two immunoglobulin molecules were used for the labeling (primary and secondary antibodies). tBid and the myc-tag have molecular weights of ~22 kD and ~67 kD, respectively. Hence, myc-tagged tBid has a size of ~5 nm. The maximal size of the tBid-immunogold complex is thus about 30 nm for 5-nm gold (10+10+5+5 nm). Hence the distance between gold and contact site is not expected to be much less than this value. With this understanding, one can see that experimental means of 23–31 nm, shown in table 1, are reasonable values for specific association of tBid with contact sites. This is especially true upon comparing with the mean distances of 70–129 nm from the random placement of gold. Thus, this nearest neighbor statistic provides strong evidence that tBid associates with mitochondrial contact sites.

## Discussion

Mitochondria are compartmentalized into three spaces by their inner and outer membranes [17]. The outer membrane surrounds the mitochondria and separates it

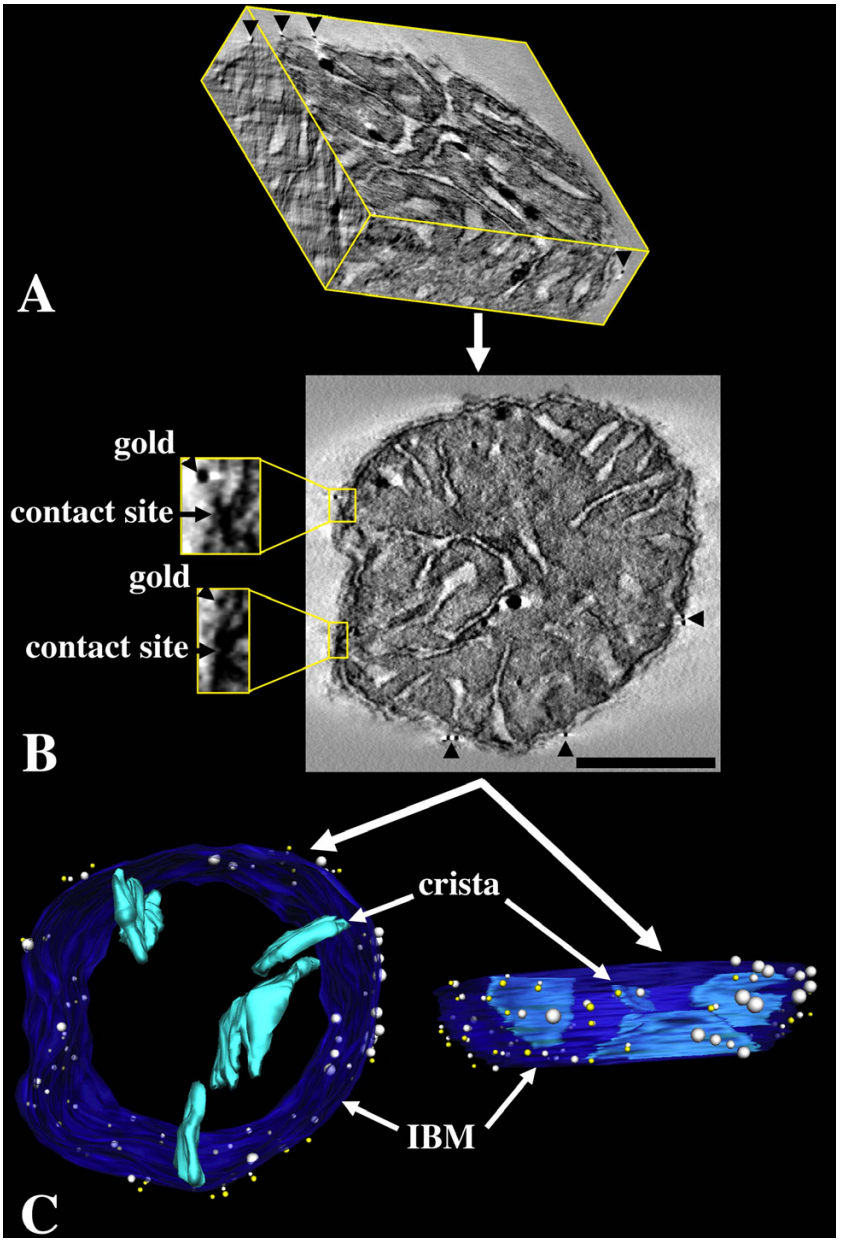


**Figure 3**
Elements of a tomographic reconstruction of a $tBid_{G94E}$-labeled mitochondrion highlight the association of tBid with contact sites. **a)** Portion of the tomographic volume sliced in three perpendicular planes. Thick sections were examined by intermediate voltage electron microscopy and were used to generate reconstructions of the immunogold-labeled outer membrane. The visualization tool ANALYZE allows the tomographic volume to be rotated and resectioned along any axis, thereby revealing both internal and surface structures along with the gold labels; it also provides the ability to correlate 2-D and 3-D views of the same region or substructure. Three-dimensional perspectives allowed us to track features, such as gold particles (arrowheads), along perpendicular faces.**b)** Slice through the volume. Several gold particles are visible (arrowheads) in this 2 nm slice, including two closely associated with contact sites (insets; 3x magnification) The scale bar = 500 nm and applies to all panels. **c)** Perpendicular views of the surface-rendered volume with selected components segmented. The visualization tool SYNU allows the surface-rendered volume to be viewed in any orientation. For clarity in visualizing the contact sites (white spheres) and gold particles (yellow spheres), the outer membrane is not shown. The inner boundary membrane (IBM) is shown in dark blue and was segmented separately from individual cristae (light blue). Only four cristae are shown to demonstrate the lamellar architecture common in liver mitochondria. Where gold particles were aggregated, only one particle is shown. The IBM was made translucent in order to visualize the cristae.

**Table 1: Distance from immunogold particles to the nearest contact site in tomographic reconstructions of liver mitochondria**

| Labeling type on Mitochondrion | Mean distance experimental (nm)[a] | Mean distance random (nm)[a,b] | Number of contact sites | Number of immunogold particles |
|---|---|---|---|---|
| WT tBid 1 | 53 ± 27 | 122 ± 56 | 39 | 23 |
| GE tBid 1[c] | 30 ± 14 | 70 ± 28 | 62 | 37 |
| GE tBid 2 | 29 ± 12 | 129 ± 76 | 13 | 5 |
| GE tBid 3 | 31 ± 6 | 77 ± 25 | 17 | 7 |
| GE tBid 4 | 23 ± 9 | 104 ± 48 | 19 | 7 |

[a]Mean ± standard deviation. Number of nearest neighbor measurements = number of immunogold particles. [b]Positions corresponding to gold particles were randomly placed around the outer membrane for each mitochondrial tomographic reconstruction according to the number of immunogold particles found in each mitochondrion (last column) and the Euclidean distance from these loci to the nearest empirical contact site was measured. [c]Note that "WT tBid 1" and "GE tBid 1" have larger number of contact sites and gold particles because more of the mitochondrial volume was found in these particular thick sections. The other three mitochondria had smaller portions sliced in their respective sections.

from the cytosol. The inner and outer membranes unite to form mitochondrial contact sites with protein composition that is still being defined [18]. It is important to test association of tBid with contact sites using electron microscopy because whereas purification schemes are based on assumptions about what contact sites should contain (and sometimes arrived at close to 100 proteins), these sites have always been defined structurally. As previously noted, contact sites are purported to have a unique lipid environment that is rich in cardiolipin. The presence of cardiolipin has been implicated in the function of numerous mitochondrial proteins including, sites I and III of the electron transport chain, the adenine nucleotide transporter, the protein translocation machinery, and the localization of mitochondrial creatine kinase [19–22].

$tBid_{G94E}$ was used predominantly for testing the hypothesis of localization of tBid to contact sites. Although this mutant translocates to mitochondria as efficiently as does the WT with diminished disruptive effect on the outer membrane, it seems conceivable that tBid harbors two distinct signals, one for translocation to mitochondria, and the other for interaction with proteins or lipids to exert its pro-apoptotic function. Disruption of this latter signal via mutation might alter tBid's submitochondrial localization, while preserving the outer membrane. We showed that WT tBid was not randomly localized with respect to contact sites. The mean experimental distance between gold particles and contact sites (53 nm; see table 1), though, was significantly higher than those values for $tBid_{G94E}$ (23–31 nm; table 1). This increased distance for WT tBid is likely due to two factors that affect the visualization of contact sites. First, tBid may have degraded the outer membrane, so that the nearest contact site is not always recognized as such. Second, the streaking caused by reconstructing the 10-nm gold particles used for WT tBid labeling may have obscured the nearest contact site in a few instances. Hence, whereas our analysis cannot disprove the hypothesis that by mutating tBid its submitochondrial localization was changed, it seems more likely that the greater value for WT tBid is caused by the factors mentioned above. Thus, it appears that the conclusion of tBid localization to contact sites can be applied more generally than the narrow interpretation of $tBid_{G94E}$ localization only.

Truncated Bid, as other BH3-only proteins, requires another protein such as Bax or Bak to exert its pro-apoptotic function [23,24]. Interestingly, tBid was found associated with mitochondrial contact sites (Figs. 1 and 2) and was shown to destabilize lipid membranes in vitro (along with Bax) by increasing the permeabilization of artificial liposomes [25,26]. Therefore it is possible that tBid can bind to the cardiolipin rich contact site membranes and destabilize them by inducing Bax or Bak to oligomerize. The membrane destabilization may cause a secondary effect of inhibiting the action of the proteins located there. This hypothesis would account for how tBid affects the function of many different processes without binding directly to several proteins. Indeed it was found that the targeting of tBid to mitochondria-like membranes occurs in the absence of proteins, yet depends upon cardiolipin being in a possibly unique structure as opposed to free cardiolipin [9]. The requirement for a specific cardiolipin structure that is likely defined by the contact site is consistent with our observation that no gold particles were found in regions stripped of the outer membrane exposing the cardiolipin-rich inner membrane.

After the induction of apoptosis, mitochondria display two distinct phases of damage. Early in the process the outer membrane becomes permeable, without rupture (Although this is controversial [27].), to several proteins found in the mitochondrial inner membrane space in-

cluding cytochrome c, in which contact sites have a probable role [28]. During this early phase, though, the inner membrane remains intact and mitochondria still retain their protein import machinery [29]. Later in the process there is swelling and herniation of the matrix leading to a distension of the cristae [8,30].

Many factors could contribute to the structural changes observed in mitochondria. tBid and other pro-death proteins such as Bax or Bak could destabilize the membrane leading to the observed changes. Additionally loss of contact site and inner membrane integrity could indirectly cause alterations in ion exchange and lead to the flow of water into the matrix. The loss of cytochrome c causes a break in the electron transfer chain resulting in the production of reactive oxygen species [31]. Reactive oxygen species are known to cause the oxidation and loss of function of many lipids including cardiolipin [20]. Finally, caspases activated downstream of cytochrome c release have been implicated in mitochondrial damage [29]. It appears likely that the cumulative damage of these agents could lead to the irreversible loss of mitochondrial membrane integrity and structure.

## Conclusions

In conclusion, we have combined the techniques of immunogold microscopy and electron tomography to determine visually and by statistical analysis that tBid is preferentially concentrated at contact sites rather than being randomly distributed along the outer membrane. For the first time, immunogold electron tomography permitted a quantitative demonstration of 3-D organellar protein labeling with antibodies. The method described is envisioned to broaden biological applications of ultrastructural immunogold labeling techniques especially in investigations dealing with compartmentalization of functional elements. For example, many organelles, including the nucleus, endoplasmic reticulum, and Golgi apparatus, have a complex organization with a unique distribution of proteins throughout each. Immunoelectron tomography is starting to be a useful tool in determining how the distribution of proteins may provide clues as to their targets or scope of action [32].

## Materials and Methods

### *Generation of Bid and caspase 8 proteins*

Full length human Bid and caspase 8 cDNA were obtained as described (Luo et al 1998). A three myc-tag recognizing the sequence EQKLISEEDL was placed into position 67 in the cDNA of full length Bid. A point mutation changing glycine 94 to glutamic acid was made into three-myc Bid using the primers 5'-GCCCAGGTCGAGGACAGCATG-3' and 5'-CATGCTGTCCTCGACCTGGGC-3' using standard techniques. Both vectors were confirmed by DNA sequencing. Bacterially expressed proteins were made as previously described [3].

### *Preparation of mitochondria for immunogold electron microscopy*

Mouse liver mitochondria were prepared fresh and treated with 1 ng myc-tagged $tBid_{G94E}$/ 100 μg of mitochondrial protein. Mitochondria were then washed 2X in mitochondria isolation buffer (MIB, 250 mM mannitol, 5 mM HEPES pH 7.2, 0.5 mM EGTA, and 0.1% (w/v) bovine serum albumin) and weakly fixed with fresh 1% paraformaldehyde in MIB for 15 min on ice. Mitochondria were pelleted (in all steps at 10,000 x g for 3 min at 4°C) and resuspended in blocking buffer (1% bovine serum albumin, 1% normal goat serum, 1% cold water fish gelatin, 0.04% glycine in MIB) for 15 min on ice. They were then pelleted and resuspended in working buffer (blocking buffer diluted 10 x in MIB) containing the primary antibody, anti-myc (1:1000) for 1 hr on ice. The no-primary control omitted the previous step only. A second control consisted of replacing the primary antibody with an excess of $tBid_{G94E}$ and continuing as with the primary antibody. Mitochondria were washed 4 x 4 min in working buffer and incubated with the indicated anti-mouse secondary antibody conjugated to 10-nm (used for wild-type tBid) or to 5-nm (used for $tBid_{G94E}$) gold beads (1:50 Amersham) for 1 hr on ice in working buffer. Subsequently, they were washed 4 x 4 min with working buffer to remove unbound secondary antibody and rinsed 1 x in cacodylate buffer (0.1 M sodium cacodylate. Electron Microscopy Sciences, Ft. Washington, PA).

Mitochondria were centrifuged and the pellet was kept intact for all remaining steps. The mitochondrial pellets were fixed in 2% glutaraldehyde in cacodylate buffer for one hour on ice and rinsed 3 x 4 min in cacodylate buffer. The mitochondrial pellets were incubated with 1% osmium tetroxide (Electron Microscopy Sciences) in cacodylate buffer for one hour on ice, followed by rinsing 3 x 4 min in ice-cold double-distilled water. The pellets were dehydrated using a successive ethanol series of 20, 50, 70, and 90% in double distilled water for 10 min each on ice. The pellets were further dehydrated at room temperature 2 x in 100% ethanol for 5 min and 2 x in 100% acetone for 5 min each.

Pellets were transferred to glass scintillation vials for resin (Durcupan ACM, EMS) infiltration. The pellets were first incubated in a sequence of 70% ethanol/30% resin, 50% ethanol/50% resin, and 30% ethanol/70% resin for 30 min each at room temperature. Pellets were then infiltrated 3 x 1 hr in 3 ml of 100% resin. After the final incubation, the resin-infiltrated pellet plus excess resin were poured into aluminum dishes and polymerized at 60°C for 36 hr.

### *Electron microscopy and tomographic reconstructions*

Tomographic reconstructions were performed as described previously [13]. Briefly, thin-sectioned material (~80-nm thick) was examined using a JEOL 1200FX electron microscope. Thick-sectioned material was examined with a JEOL 4000EX microscope operating at 400 keV. The 0.75 μm thick sections were tilted through 120° of rotation, and electron micrographs were taken in 2° increments. Using the SUPRIM software package, Four tilt series from different sections consisting of 61 tilt images each were then digitized, aligned, and back projected using R weighting to generate the volume information. Volume segmentation of the reconstructed mitochondria using Xvoxtrace software was used to delineate the inner boundary membrane, cristae, outer membrane, contact sites, and gold particles. This information was used to construct surface-rendered computer graphic representations using the SYNU software package. Gold particles were represented by gold spheres in the surface-rendered volume.

### *Statistical analysis*

To determine whether immunogold-labeled tBid is spatially clustered or randomly located about contact sites, a spatial point pattern statistics was used, namely, the nearest neighbor statistic [16]. The Euclidean distances from each immunogold particle to all of the contact sites in the reconstruction was calculated for all the particles using a similar approach to that described by Perkins and coworkers [13]. The nearest neighbor statistic was calculated for the reconstruction using the closest observed contact site to each gold particle and then calculating the mean and standard deviation for all such measurements in a reconstructed mitochondrion. These values were compared with those derived from simulations in which the same number of gold particles determined empirically were randomly placed on the mitochondrial surface.

## Abbreviations

MIB – Mitochondrial Isolation Buffer

SDS – PAGE-Sodium Dodecylsulfate-Polyacrylamide Gel Electrophoresis

tBid – Truncated Bid, the C-terminal portion of Bid after cleavage by caspase-8.

$tBid_{G94E}$ – A point mutation changing glycine 94 to glutamic acid in three-myc Bid.

## Acknowledgements

We thank the reviewers and Tom Deerinck for their helpful comments. X.W. was supported by Grant #0050769Y. Part of this work was performed at the National Center for Microscopy and Imaging Research supported by NIH Research Resource Grant # RR04050 to M. H. Ellisman and NIH grants R01 NS 14718 to MHE and P01 KD54441 to S. S. Taylor.

## References

1. Vander Heiden MG, Thompson CB: **Bcl-2 proteins: regulators of apoptosis or of mitochondrial homeostasis?** *Nat Cell Biol* 1999, **1**:E209-216
2. Li H, Zhu H, Xu C, Yuan J: **Cleavage of Bid by caspase 8 mediates the mitochondrial damage in the Fas pathway of apoptosis.** *Cell* 1998, **94**:491-501
3. Luo X, Budihardjo I, Zou H, Slaughter C, Wang X: **Bid, a Bcl-2 interacting protein, mediates cytochrome c release from mitochondria in response to activation of cell surface death receptors.** *Cell* 1998, **94**:481-490
4. Du C, Fang M, Li Y, Li L, Wang X: **Smac, a mitochondrial protein that promotes cytochrome c-dependent caspase activation by eliminating IAP inhibition.** *Cell* 2000, **102**:33-42
5. Li LY, Luo X, Wang X: **Endonuclease G is an apoptotic DNAse when released from mitochondria.** *Nature* 2001, **412**:95-99
6. Vander Heiden MG, Chandel NS, Schumacker PT, Thompson CB: **Bcl-XL prevents cell death following growth factor withdrawal by facilitating mitochondrial ATP/ADP exchange.** *Molecular Cell* 1999, **3**:159-167
7. Vander Heiden MG, Li XX, Gottlieb E, Hill RB, Thompson CB, Colombini M: **Bcl-xL promotes the open configuration of the voltage-dependent anion channel and metabolite passage through the outer mitochondrial membrane.** *J Biol Chem* 2001, **276**:19414-19419
8. Mootha VK, Wei MC, Buttle KF, Scorrano L, Panoutsakopoulou V, Mannella CA, Korsmeyer SK: **A reversible component of mitochondrial respiratory dysfunction in apoptosis can be rescued by exogenous cytochrome c.** *EMBO J* 2001, **20**:661-671
9. Lutter M, Fang M, Luo X, Nishijima M, Xie X, Wang X: **Cardiolipin provides specificity for targeting of tBid to mitochondria.** *Nature Cell Biol* 2000, **2**:754-761
10. Ardail D, Privat J, Egret-Charlier M, Levrat C, Lerme F, Louisot P: **Mitochondrial Contact Sites.** *J Biol Chem* 1990, **265**:18797-18802
11. Perkins G, Frey T: **Electron tomography** *In: Encyclopedia of Molecular Biology. (Edited by Creighton T). New York, John Wiley & Sons* 1999796
12. Frey TG, Mannella CA: **The internal structure of mitochondria.** *TIBS* 2000, **25**:319-324
13. Perkins G, Renken C, Martone M, Young S, Ellisman MH, Frey TG: **Electron tomography of neuronal mitochondria: 3-D structure and organization of cristae and membrane contacts.** *J Struct Biol* 1997, **119**:260-272
14. Perkins G, Frey T: **Recent structural insights into mitochondria obtained by microscopy.** *Micron* 2000, **31**:97-111
15. Perkins G, Renken C, Song JY, Young S, Lamont S, Martone M, Lindsey S, Frey TG, Ellisman MH: **Electron tomography of large, multicomponent biological structures.** *J Struct Biol* 1997, **120**:219-227
16. Boots BN, Getis A: **Point Pattern Analysis.** *Newbury Park, Sage* 1988
17. Lehninger AL, Nelson DL, Cox MM: **Principles of Biochemistry.** *New York, Worth Publishers* 1993
18. Crompton M: **Mitochondrial intermembrane junctional complexes and their role in cell death.** *J Physiol* 2000, **529**:11-21
19. Chen JJ, Bertrand H, Yu BP: **Inhibition of adenine nucleotide translocator by lipid peroxidation products.** *Free Radical Biol Medicine* 1995, **19**:583-590
20. Hoffmann B, Stockl A, Schlame M, Beyer K, Klingenberg M: **The reconstituted ADP/ATP carrier activity has an absolute requirement for cardiolipin as shown in cysteine mutants.** *J Biol Chem* 1994, **269**:1940-1944
21. Muller M, Moser R, Cheneval D, Carafoli E: **Cardiolipin is the membrane receptor for mitochondrial creatine phosphokinase.** *J Biol Chem* 1985, **260**:3839-3843
22. Weiss C, Oppliger W, Vergeres G, Demel R, Jeno P, Horst M, De Kruijff B, Schatz G, Azem A: **Domain structure and lipid interaction of recombinant yeast Tim 44.** *Proc Natl Acad Sci USA* 1999, **96**:8890-8894
23. Wei MC, Zong WX, Cheng EH, Lindsten T, Panoutsakopoulou V, Ross AJ, Roth KA, MacGregor GR, Thompson CB, Korsmeyer SJ: **Proapoptotic Bax and Bak: A requisite gateway to mitochondrial dysfunction and death.** *Science* 2001, **292**:727-730
24. Zong WX, Lindsten T, Ross AJ, MacGregor GR, Thompson CB: **BH3-only proteins that bind pro-survival Bcl-2 family mem-**

**bers fail to induce apoptosis in the absence of Bax and Bak.** *Genes Dev* 2001, **15**:1481-1486
25. Basanez G, Nechushtan A, Drozhinin O, Chanturiya A, Choe E, Tutt S, Wood KA, Hsu Y, Zimmerberg J, Youle RJ: **Bax, but not Bcl-xL, decreases the lifetime of planar phospholipid bilayer membranes at subnanomolar concentrations.** *Proc Natl Acad Sci USA* 1999, **96**:5492-5497
26. Kudla G, Montessuit S, Eskes R, Berrier C, Martinou J, Ghazi A, Antonsson B: **The destabilization of lipid membranes induced by the c-terminal fragment of caspase-8 cleaved Bid is inhibited by the n-terminal fragment.** *J Biol Chem* 2000, **275**:22713-22718
27. Bernardi P, Petronilli V, Di Lisa F, Forte M: **A mitochondrial perspective on cell death.** *Trends Biochem Sci* 2001, **26**:112-117
28. Doran E, Halestrap AP: **Cytochrome c release from isolated liver can occur independently of outer-membrane rupture: Possible role of contact sites.** *Biochem J* 2000, **348**:343-350
29. Von Ahsen O, Renken C, Perkins G, Kluck RM, Bossy-Wetzel E, Newmeyer DD: **Preservation of mitochondrial structure and function after Bid- or Bax-mediated cytochrome c release.** *J Cell Biol* 2000, **150**:1027-1036
30. Vander Heiden MG, Chandel NS, Williamson EK, Schumacher PT, Thompson CB: **Bcl-XL regulates the membrane potential and volume homeostasis of mitochondria.** *Cell* 1997, **91**:627-637
31. Cai J, Jones DP: **Mitochondrial generation triggered by cytochrome c loss.** *J Biol Chem* 1998, **273**:11401-11404
32. Shoop RD, Martone ME, Yamada N, Ellisman ME, Berg DK: **Neuronal acetylcholine receptors with $\alpha$7 subunits are concentrated on somatic spines for synaptic signaling in embryonic chick ciliary ganglia.** *J Neurosci* 1999, **19**:692-704
33. Hackenbrock CR: **Chemical and physical fixation of isolated mitochondria in low-energy and high-energy states.** *Proc Natl Acad Sci USA* 1968, **61**:598-605